Experimental study on mode instabilities in all-fiberized high-power fiber amplifiers

Rumao Tao (陶汝茂), Pengfei Ma (马鹏飞), Xiaolin Wang (王小林)*, Pu Zhou (周 朴), and Zejin Liu (刘泽金)**

College of Optoelectronic Science and Engineering, National University of Defense Technology, Changsha 410073, China

**Corresponding authors: chinawxllin@163.com; **corresponding author: zhoupu203@163.com*

Received March 17, 2014; accepted May 3, 2014; posted online October 15, 2014

We report the experimental study on mode instabilities (MI) in large mode area step-index fibers by testing a 30/400 μm step-index fiber in a single-pass co-pumped all-fiberized amplifier, delivering up to ~550 W of extracted output power without MI. The pump power is increased well above the MI threshold to study the temporal dynamics of MI in detail, which are characterized by using both high-speed camera measurement with ~2200 frames per second and photodiode traces. The experimental results are compared with the theoretical results. The MI frequency component is seen to appear on top of system noise, such as electric noise, which shows that system noise may influence the onset of MI. The beam quality of the fiber amplifier is measured, which is ~1.4 before the onset of MI, and degrades gradually to ~2.1 after the onset of MI.

OCIS codes: 190.3100, 060.2320, 140.6810.
doi: 10.3788/COL201412.S20603.

With the impressive development of high brightness diode pump technology and large mode area (LMA) double-clad fiber craft in recent years, fiber laser systems have rapidly evolved into light sources able to deliver single-mode output powers beyond 10-kW level[1], the unwanted nonlinear effects in which are reduced by increasing the mode field areas. However, LMAs, with the current technological limitations, inevitably result in multimode operation, which combining with high-average power operation has resulted in a new effect called mode instabilities (MI)[2], the onset of which currently limits the further power scaling of Yb-doped fiber laser systems with diffraction-limited beam quality. Due to the far-reaching impact of MI, the first report of this phenomenon triggered the publication of several further articles dealing with it experimentally and theoretically[3–14]. However, most of the experimental study is carried out on photonic crystal fiber in counter-pumped spatial structure, and few work on co-pumped all-fiberized laser systems based on step-index fiber has been reported, which is different in mode character and heat dissipating performance, and is the main configuration of the commercial high-power fiber laser system. In addition, step-index fiber has simple structure and can be compared with theoretical model directly.

Here we report the experimental study on MI in LMA step-index fibers by testing a 30/400 μm step-index fiber in a single-pass co-pumped all-fiberized amplifier. Temporal and frequency dynamics of MI are investigated in detail, which is compared with the results obtained by theoretical model.

Figure 1 depicts the experimental setup. The broadband continuous wave seed laser provided about 20 mW seed power with central wavelength of 1064 nm. A three-stage preamplifier is developed to boost the average power to about 20 W. The main amplifier was based on LMA double-clad ytterbium-doped fiber (YDF) with core diameter of 30 μm (core NA = 0.06) and cladding diameter of 400 μm. The YDF was coiled with a diameter of ~25 cm and placed on an aluminum heat sink to ensure sufficient cooling. Six multimode fiber pigtailed 976-nm LDs are used to pump the gain fiber through a (6+1)×1 signal/pump combiner. The output end of the YDF is angle cleaved and the output laser was collimated to about 7 mm in diameter. The measurement system is composed of low-speed and high-speed cameras, an M^2 analyzer, and a photoelectric detector (PD), which is not shown.

We have used two types of cameras to study the MI spatially: a low- and a high-speed camera. The first one is able to capture ~8 images per second while the second one is a high-speed camera which can capture ~2200 frames per second. Figures 2(a) and (b) show

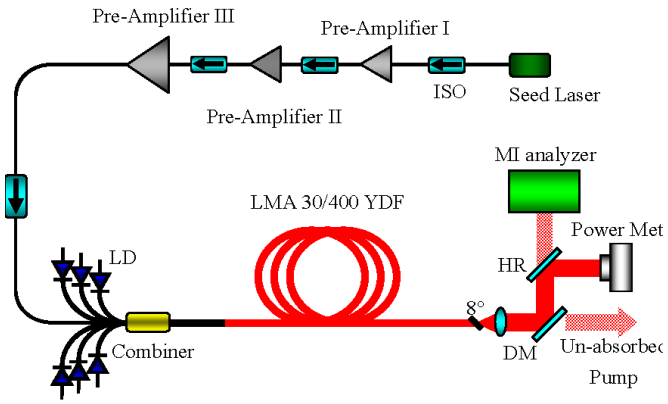

Fig. 1. Experimental setup of the fiber amplifier.

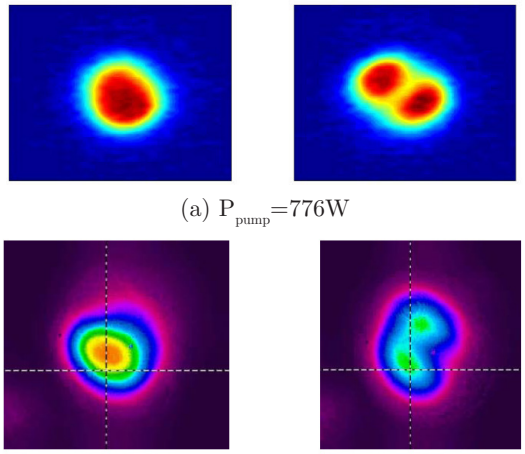

(a) P_{pump}=776W

(b) P_{pump}=1080W

Fig. 2. Far-field intensity distributions captured from (a) the high-speed (Media 1) and (b) the low-speed cameras.

far-field intensity from the low-speed and high-speed cameras, respectively. Media 1 (Fig. 2(a)) shows the recorded high-speed video of the far-field beam-profile evolution within a time period of 50 ms after the onset of MI. It shows that the beam profiles fluctuate between fundamental mode and LP_{11}-like mode near the threshold power. For the low-speed camera, the fluctuation of mode became observable after the pump power was increased beyond 960 W. However, for the high-speed camera, the fluctuation of mode became observable when the pump power was increased beyond 706 W with extracted signal power of 550 W. This difference is because of the small high-order mode content at the beginning of MI and low frame frequency of the low-speed camera, resulting in the long-time average of beam-profile fluctuation. The beam quality of the output beams has been measured. At pump power of 636 W, the beam quality of the fiber laser is about 1.4 (M^2), which degrades gradually after the onset of MI and is 2.2 at pump power of 1230 W.

To study the temporal dynamics in detail, we used a simple photodiode measurement of a portion of the transversal beam profile, which provided important characteristics of the temporal dynamics such as their temporal periodicity or noise. A PD with a hole of 1.5 mm diameter was put in the center of the collimated beam to detect the temporal character of the MI. The time traces at four different pump power levels are shown in Fig. 3. It can be seen that, before the onset of MI (see Fig. 3(a)), the time trace is noise-like while the time traces have a periodic saw-tooth-like oscillation on millisecond timescale after the onset of MI as shown in Figs. 3(b) and (c). With increasing pump power, the period of the fluctuations becomes short (see Fig. 3(c)), which indicates higher order modes set in, and periodic behavior becomes invisible (see Fig. 3(d)) with further pump power scaling.

Furthermore, we applied Fourier analysis on the time traces to calculate the corresponding Fourier spectra (FS) to simplify the study on the periodicity of the time traces. FS under different pump power levels are shown in Fig. 4, which reveal the increase in instability. It can be seen that with increasing pump power more energy is distributed to higher frequency components, that is, the spectrum broadens: in the stable regime, the frequency components of the fluctuations

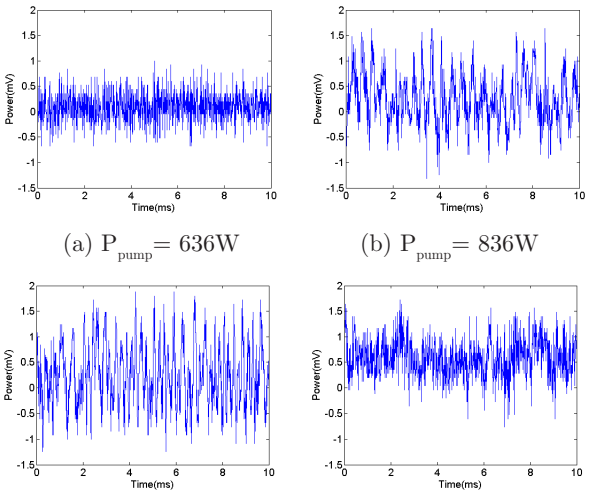

(a) P_{pump}= 636W (b) P_{pump}= 836W

(c) P_{pump}= 1020W (d) P_{pump}= 1230W

Fig. 3. Time traces of MI at different pump power levels.

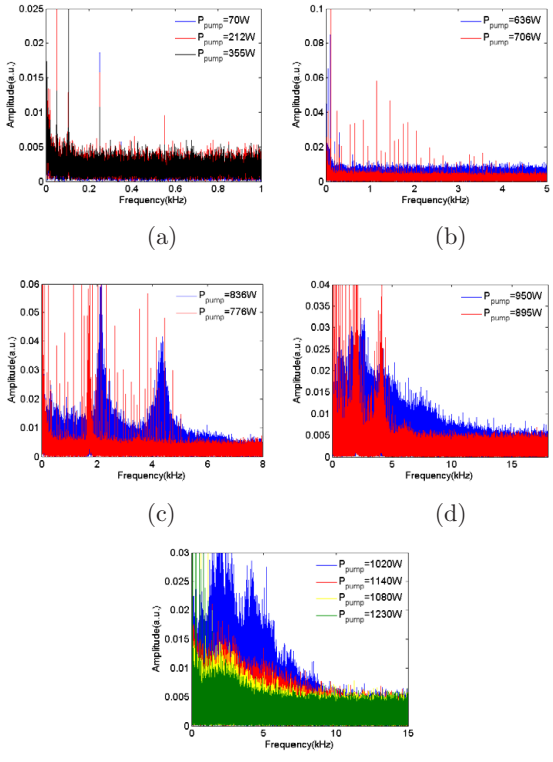

(a) (b)

(c) (d)

(e)

Fig. 4. FS of the temporal power evolution under different pump power levels.

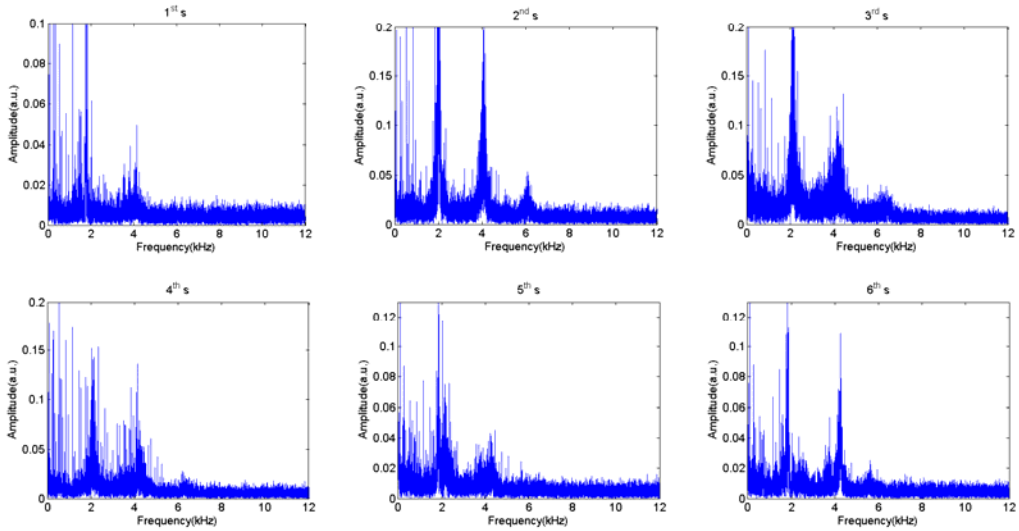

Fig. 5. FS of the temporal power evolution at different times.

are distributed in the range of 0–1 kHz. Near the onset of MI, the sign of instability appeared with discrete frequency peaks in 0–5 kHz showing up the frequency space of which is the integral multiple of 50 Hz and clearly means the MI is related to system-dependent noise, such as electrical noise. In the transition regime, resonances with certain bandwidth, the higher harmonics of which showed up with pump power scaling, showed up on top of suspected electrical-noise-induced frequency peaks, and the center frequency of the resonances shifts to the higher frequency with increasing pump power. With further increasing pump power and running into the chaotic regime, the bandwidth of the resonances broadens and the energy spread over a wide frequency range up to 15 kHz with original resonances is being weakly seen in some areas. With further pump power scaling in chaotic regime, the power in higher frequency components becomes less, which means the spectrum has been compressed.

To study the temporal character of the FS, we calculated the FS of the time traces at different times. We recorded time traces of 6 s at pump power of 895 W in transition regime and calculated the FSs of every second, which is shown in Fig. 5. It shows that the frequency component changes with time: a clear frequency component of ~2 kHz with also higher harmonics of that component at ~4 and ~6 kHz can be seen at one time while only one higher harmonic at 4 kHz can be observed at other time. It should be noted that discrete frequency peaks with frequency space being integral multiple of 50 Hz appears as background in all the FSs of Figs. 4 and 5.

Based on the semi-analytic model[8,13], the nonlinear coupling coefficient χ and quantum-noise-induced threshold power of the fiber have been calculated, which is presented in Fig. 6. The calculation parameters of the fiber is taken the same as that used in the experiment with core refractive index $n_c = 1.45$, convection coefficient $h_q = 1000$ W/(m^2 K), thermo-optic coefficient $\eta = 1.2\times10^{-5}$ K^{-1}, thermal conductivity $\kappa = 1.38$ W/(m K), and $\rho C = 1.67\times10^6$ J/(m^3 K). Figure 6(a) clearly shows that the nonlinear gain of the LP_{01}—LP_{02} /LP_{21}/LP_{31} coupling is much less than that for the LP_{01}—LP_{11} coupling in this case. The maximal coupling occurs at ~3 kHz for the LP_{01}—LP_{11} coupling, which is larger than the experimental measured value. This may be because the simplified model assumes that the heat profile mimics the irradiance profile and ignore the influence of transverse hold burning (THB). By taking the effect of THB into consideration, the maximal coupling frequency shifts to the lower frequency[15]. High-order mode fraction ζ as a function of output signal power P_1 is plotted in Fig. 6(b). The threshold power of quantum-noise-induced MI is calculated to be 860 W, which is higher than the experimental result of 550 W. The system noise, such as electric noise shown in Figs 4 and 5, is suspected to be the reason for decreasing threshold power[5].

In conclusion, we report the experimental study on MI in LMA step-index fibers by testing a step-index fiber in a single-pass co-pumped all-fiberized amplifier,

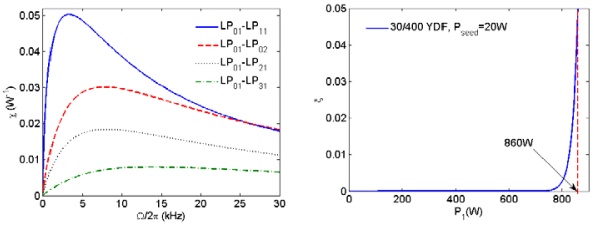

(a) χ as a function of Ω (b) ζ as a function of output signal power

Fig. 6. Theoretical calculation results of 30/400 YDF.

delivering up to ~550 W of extracted output power without MI. The pump power is increased well above the MI threshold to study the dynamics of MI, which are characterized spatially, temporally, and frequencially by using both cameras and photodiode. Based on the far-field beam profiles recorded by high-speed camera, the beam profiles fluctuate rapidly after the onset of MI. The beam profiles fluctuate between the fundamental mode and the LP_{11} mode near the threshold power. The beam quality of the fiber amplifier is measured. The M^2 value of the amplifier is ~1.4 before the onset of MI, and degrades gradually to ~2.2 after the onset of MI. Based on the photodiode traces and Fourier analysis, frequency dynamics of MI are investigated in detail. Frequency component of ~2 kHz also with higher harmonics of that component at ~4 kHz and ~6 kHz has been observed, and the frequency component changes with time while the center frequency of the resonances varies with pump power. In addition, the MI frequency component is seen to appear on top of system noise, such as electric noise. The experiment results are compared with the theoretical results.

The authors thank Chen Shi, Hanwei Zhang and Hailong Yu for providing helpful assistance in carrying out the experiments. This work was supported by the Program for New Century Excellent Talents in University, the National Science Foundation of China (No. 61322505), the Hunan Provincial Innovation Foundation for Postgraduate (No. CX2012B035), and the Innovation Foundation for Excellent Graduates in National University of Defense Technology (No. B120704).

References

1. E. Stiles, in *Proceedings of 5th International Workshop Fiber Lasers* (2009).
2. T. Eidam, C. Wirth, C. Jauregui, F. Stutzki, F. Jansen, H. J. Otto, O. Schmidt, T. Schreiber, J. Limpert, and A. Tünnermann, Opt. Express **19,** 13218 (2011).
3. H. J. Otto, F. Stutzki, F. Jansen, T. Eidam, C. Jauregui, J. Limpert, and A. Tünnerman, Opt. Express **20,** 15710 (2012).
4. B. Ward, C. Robin, and I. Dajani, Opt. Express **20,** 11407 (2012).
5. M. M. Johansen, M. Laurila, M. D. Maack, D. Noordegraaf, C. Jakobsen, T. T. Alkeskjold, and J. Lægsgaard, Opt. Express **21,** 21847 (2013).
6. C. Jauregui, T. Eidam, J. Limpert, and A. Tünnermann, Opt. Express **19,** 3258 (2011).
7. A. V. Smith and J. J. Smith, Opt. Express **19,** 10180 (2011).
8. K. R. Hansen, T. T. Alkeskjold, J. Broeng, and J. Lægsgaard, Opt. Express **21,** 1944 (2013).
9. A. V. Smith and J. J. Smith, Opt. Express **20,** 24545 (2012).
10. L. Dong, Opt. Express **21**, 2642 (2013).
11. H. J. Otto, C. Jauregui, F. Stutzki, F. Jansen, J. Limpert, and A. Tünnermann, Opt. Express **21,** 17285 (2013).
12. X. Wang, R. Tao, H. Xiao, P. Zhou, C. Zhang, and X. Xu, in *Proceedings of Advanced Solid State Lasers Congress* JTh2A. 44 (2013).
13. R. Tao, X. Wang, H. Xiao, P. Zhou, and Z. Liu, Acta Opt. Sin. **34,** 0114002 (2014).
14. W. Ke, X. Wang, X. Bao, and X. Shu, Opt. Express **21,** 14272 (2013).
15. A. V. Smith and J. J. Smith, "Frequency dependence of mode coupling gain in Yb doped fiber amplifiers due to stimulated thermal Rayleigh scattering," http://www.arxiv.org/abs/1301.4277 (2013).